FABRICATION AND TESTING OF A LARGE AREA, HIGH DENSITY, PARYLENE MEMS µECOG ARRAY

P. Ledochowitsch[1], R. J. Félus[2], R. R. Gibboni[1], A. Miyakawa[1], S. Bao[1] and M. M. Maharbiz[1]
[1]University of California, Berkeley, California, USA
[2]INP-PHELMA, Grenoble, FRANCE

ABSTRACT

We report the design, microfabrication and testing of a flexible 256-electrode array for micro-electrocorticography (µECoG) with an electrode pitch of 500 µm. Our µECoG grid is a flexible five-layer parylene MEMS device (two layers of platinum insulated by three layers of parylene) featuring plasma-etched vias and a monolithically integrated parylene cable which is compression-bonded to a fan-out board using anisotropic conductive film (ACF) technology. We have characterized the device by electrochemical impedance spectroscopy in artificial cerebrospinal fluid (aCSF) and recorded acoustic evoked potentials in vivo from the *rat* primary auditory cortex.

INTRODUCTION

This paper reports the design, microfabrication and testing of a flexible 256-electrode array for micro-electrocorticography (µECoG). Our µECoG grid is a flexible five-layer parylene MEMS device (two layers of platinum between three layers of parylene) featuring plasma-etched vias and a monolithically integrated parylene cable which is compression-bonded to a fan-out board using anisotropic conductive film (ACF) technology. The electrode density exceeds that of previously published µECoG devices with comparable number of electrodes by an order of magnitude [1], albeit smaller grids with similar electrode pitch have been reported in literature [2].

Electrocorticography (ECoG), i.e. the measurement of electrical potentials on the surface of the cerebral cortex, constitutes a trade-off in invasiveness and resolution between traditional scalp electroencephalography (EEG) and microelectrode recordings inside the cerebral cortex. In the 1950s Jasper and Penfield pioneered ECoG [3] for pre-surgical evaluation of patients suffering from intractable epilepsy. For this purpose spacing electrodes 1 cm apart typically provides sufficient resolution. Resent research on micro-seizures, however, implies that in fact much higher spatial resolution may be beneficial [4]. Brindley and Craggs reported a correlation between voluntary movement and ECoG signals as early as in 1972 [5]. However, only recently, the brain-machine-interface (BMI) community has demonstrated the great promise, ECoG-based BMIs [6] harbor for the neural control of high performance motor [7] and communication [8] prostheses, e.g. for locked-in

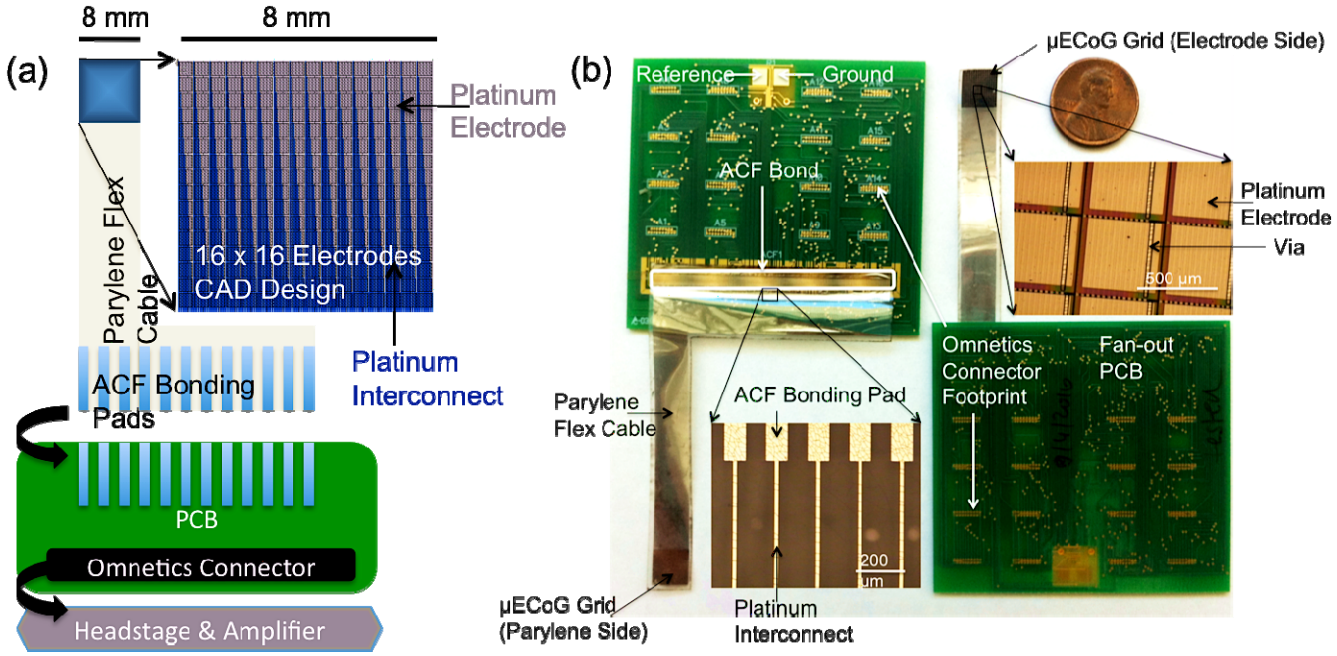

Figure 1: (a) Full system concept: the 256-electrode grid (CAD design) is monolithically integrated with the parylene cable on wafer level. The parylene cable fans out into an array of pads, which are ACF-bonded to a PCB outfitted with Omnetics connectors compatible with commercial headstages and amplifiers. (b) Annotated post-fabrication photographs show the released flexible electrode array with parylene cable ACF-bonded onto the fan-out PCB. Micrographs show the transition region between parylene cable and ACF binding pads (bottom left) and a close-up of the electrode pads including plasma-etched vias.

patients. For applications in BMI, the development of high fidelity ECoG grids with electrode size and pitch that optimizes spatiotemporal resolution and the signal-to-noise ratio (SNR) is key. There is no consensus on either optimal electrode pitch or size for µECoG. The to-date singular publication that has specifically addressed the question of optimal pitch [9], indicates that spacing electrodes on the surface of the cerebral cortex as close as 600 µm apart may not yet lead to spatial oversampling. This result is consistent with work by Katz and co-workers who showed that local field potentials (LFPs) originate from within a mere 250 µm of the recording electrode [10].

One of the major advantages of ECoG over invasive microelectrode recordings is the potential to simultaneously record from extended parts of the brain and to study synchronization and communication events [11,12]. Thus, it is not only important to increase the spatial resolution of electrocortical grids but also their areal coverage, i.e. the total number of recording sites.

DESIGN

We have designed a 256 channel µECoG with an electrode pitch of 500 µm and square electrodes 440 µm x 440 µm in size (Fig. 1). A 6 cm long parylene cable is monolithically integrated with the ECoG array on wafer level. This cable is thermo-compression-bonded to a fan-out plastic circuit board (PCB) in an anisotropic conductive film (ACF) flex process. The adaptor PCB is outfitted with 16 commercial 18-pin Omnetics connectors for compatibility with commercial neural recording headstages and amplifiers. Cable and electrode pads are routed on separate metal layers and interconnected through etched vias. This enables larger electrode pads than could be realized with a single metal layer, decreasing electrode impedance, improving the signal-to-noise ratio (SNR) and preventing spatial aliasing.

We have made a conscious choice to only make use of fully biocompatible materials that are already FDA-approved for implantation in humans: platinum and parylene C [13]. This decision does not guarantee FDA-approval but is expected to facilitate the process.

FABRICATION

Wafer level fabrication

The 5-layer devices, only 12 µm thin, were fabricated in a custom parylene MEMS process as shown in Fig. 2. A borofloat glass carrier wafer (1) was cleaned by sonication in 18 MΩ water, isopropanol (IPA) and acetone (3 min each). Parylene C (poly(para-chloro-xylelene), obtained form Specialty Coating Systems) was deposited (2) (Specialty Coating Systems Parylene Deposition System Model 2010: $T_{furnace}$ = 680 °F $T_{chamber}$= 135 °F $T_{vaporizor}$= 175 °F, p = 25 mTorr, initial dimer mass: 10 g, resulting thickness: 9 µm, thickness uniformity across wafer was ±1 µm). Platinum (obtained from Sigma-Aldrich) was deposited in a lift-off process (3): Positive photoresist (OCG 825 35CS) was spin-coated (200 RPM, 2 µm resulting

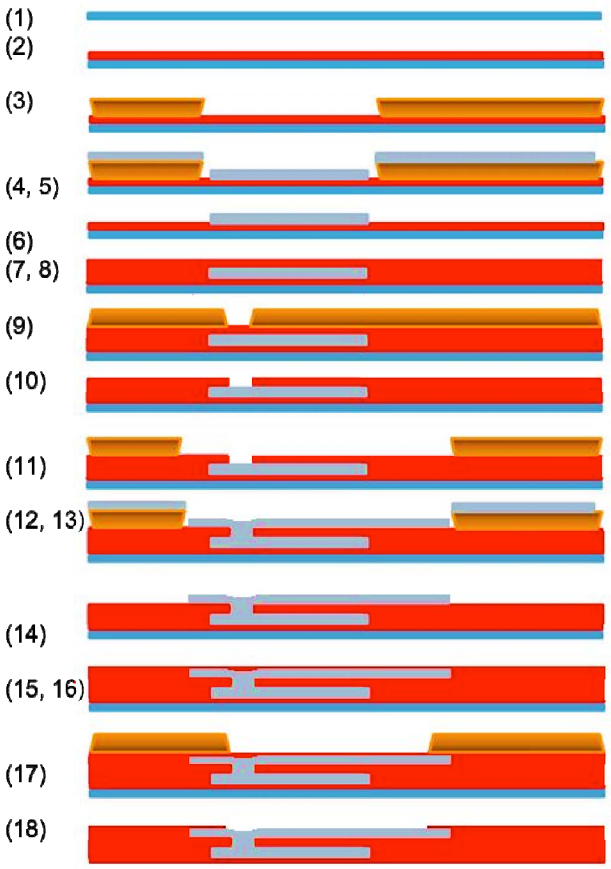

Figure 2. Custom parylene MEMS process flow: Parylene (red), platinum (gray), photoresist (orange).

thickness), soft-baked (90 s at 90 C), exposed using a Karl Suss MA6 mask aligner (multi-exposure: three 3 s intervals at 20 mW/cm^2 with 10 s breaks, post exposure bake: 120 s at 120 °C), and developed (4 x 30 s in OCG 934 2:1). Before metal deposition, the parylene surface was plasma-treated (1:1 mixture of methane and oxygen, 200 W, 56 mTorr, 30 s in Plasma-Therm PK-12 RIE) to achieve better metal adhesion (4). Platinum was e-beam-evaporated (5) (Edwards EB3: 130 nm as confirmed by profilometry using KLA-Tencor Alpha-step IQ) and lifted-off by soaking and soft scrubbing in acetone for about 15 minutes (6). A monolayer of γ-MPS (γ-methacryloxypropyltrimethoxysilane, aka A-174, a standard parylene adhesion promoter) was vapor-deposited (ASMT MVD100) (7) followed by the second layer of parylene (conditions as above, initial dimer mass: 2 g, resulting thickness approximately 1.5 µm) (8). Vias were patterned in the parylene by oxygen plasma reactive ion etching (RIE) (oxygen, 200 W, 73 mTorr, 10 x 30 s intervals with 30 s cool-down periods in Plasma-Therm PK-12 RIE) (10) through a photoresist mask (photoresist deposition, exposure and development as described above) (9). The second layer of platinum was patterned by lift-off in steps (11)-(14), identical to steps (3)-(6). A monolayer of γ-MPS was deposited (15) followed by the third and final layer of

parylene (16) as described above for steps (7) and (8). Vias establishing contact between tissue and electrodes were patterned through a PR mask (17) by RIE (18) as described in steps (9) and (10). Finally, a device outline was cut using a carbon dioxide laser cutter (Versalaser, Universal Laser, Inc.) operating in paper cutting mode and the devices were released from the glass carrier wafer in a mild solution of detergent (Triton-X).

Assembly and packagng

A fan-out PCB was designed to connect a 1D array of ACF bonding pads (100 um line width, 200 um pitch) to 16 footprints of through-hole Omnetics Nano connectors (A79014-001) using DipTrace and manufactured by Advanced Circuits.

The wafer level devices were bonded to the PCB in an ACF process. ACF (3M 5552R, 2 mm wide) was pre-bonded to the corresponding PCB footprint using an Ohashi HMB-10 table-top bonder equipped with a 2.5 mm bond head (1 s, 90 C, 5 kg/cm^2). Parylene devices were aligned by hand under a stereomicroscope and tacked to the ACF film with a soldering iron. The final bond was performed using the HMB-10 (20 s, 200 C, 40 kg/cm^2).

RESULTS

EIS characterization

We have characterized the electrode/electrolyte interface by electrochemical impedance spectroscopy (EIS) (Solartron constant-voltage mode, frequency sweep: 0.1 Hz to 10 kHz, AC-amplitude: 50 mV, open circuit potential: 265 mV). The device formed the active electrode a platinum wire the counter-electrode and a silver wire the reference electrode. We used artificial cerebrospinal fluid (aCSF, Artificial CSF Perfusion Fluid, Harvard Apparatus, ion concentrations in mM: Na 150; K 3.0; Ca 1.4; Mg 0.8; P 1.0; Cl 155) as the electrolyte.

The Nyquist plots have been fitted to a modified Randles Cell model to extract the line resistance (R_s =11.32±0.02 kΩ), charge transfer resistance (R_p =102.5±0.5 kΩ) and the parameters of the constant phase element (CPE: n=0.763±0.004; P=51.8±0.4 μF·s^n) (Fig. 3).

In vivo electrophysiological recordings

The ECoG array was tested in vivo on the auditory cortex of the rat. The University of California Berkeley Animal Care and Use Committee approved all procedures used in this study. One female Sprague Dawley rat was preanesthetized with buprenorphine (0.05 mg/kg) administered subcutaneously 30 min before anesthesia with sodium pentobarbitol (50 mg/kg for induction by intraperitoneal injection, 10-20 mg/kg supplemental as needed by intramuscular injection). Atropine (0.1 mg/kg) and dexamethasone (1 mg/kg) were injected subcutaneously. The rat was secured with a custom head holder and the cisterna magna was drained of cerebrospinal fluid to reduce brain pulsation and edema. An incision was made in the skin over the right auditory cortex, the temporalis muscle was removed, and the skull was exposed so that a wide craniotomy and durectomy could be made. Artificial CSF (same as for EIS characterization) was continuously applied to the exposed area.

We placed the electrode array on the cortex and recorded responses (sampling rate, 384 Hz) to 25-ms white noise bursts played through a custom-made tube speaker inserted into the left ear to evoke responses in the right auditory cortex. The sounds were presented at 10-dB attenuation increments between 10 dB to 80 dB attenuation in order to sample a wide range of intensities. Responses to 63-71 presentations of each intensity were averaged. We have observed acoustic evoked potentials after a characteristic delay of approximately 30 ms post-stimulus. As expected, higher stimulus levels resulted in larger potential amplitudes and slightly shorter response times. (Fig 4, a and c). As a control we have placed the μECoG array on the brain approximately 5 mm anterior to auditory cortex. As expected, no acoustic evoked potential has been observed in the control experiment (Fig. 4, b and d). Sound stimuli were generated using Cool Edit Pro (Syntrillium, 97656 Hz sampling rate) and a Tucker-Davis Technologies system (TDT System 3) was used for speaker calibration, sound delivery (through a STAX speaker), and electrophysiological recording.

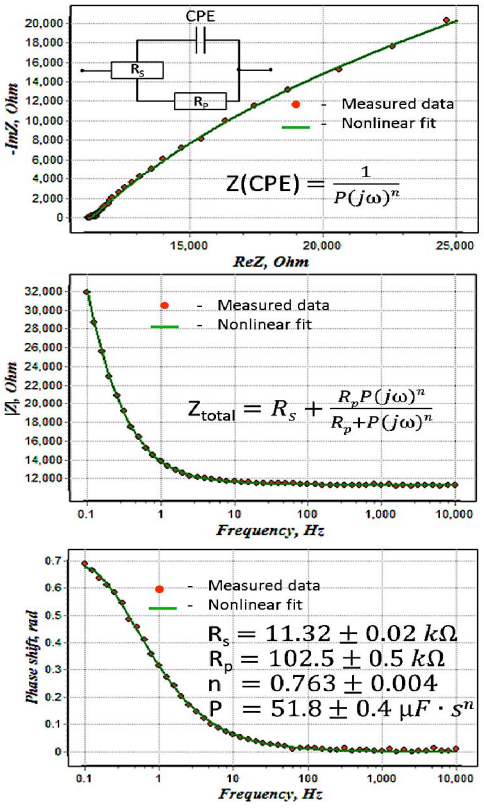

Figure 3. Characterization of electrode-electrolyte interface by electrochemical impedance spectroscopy.

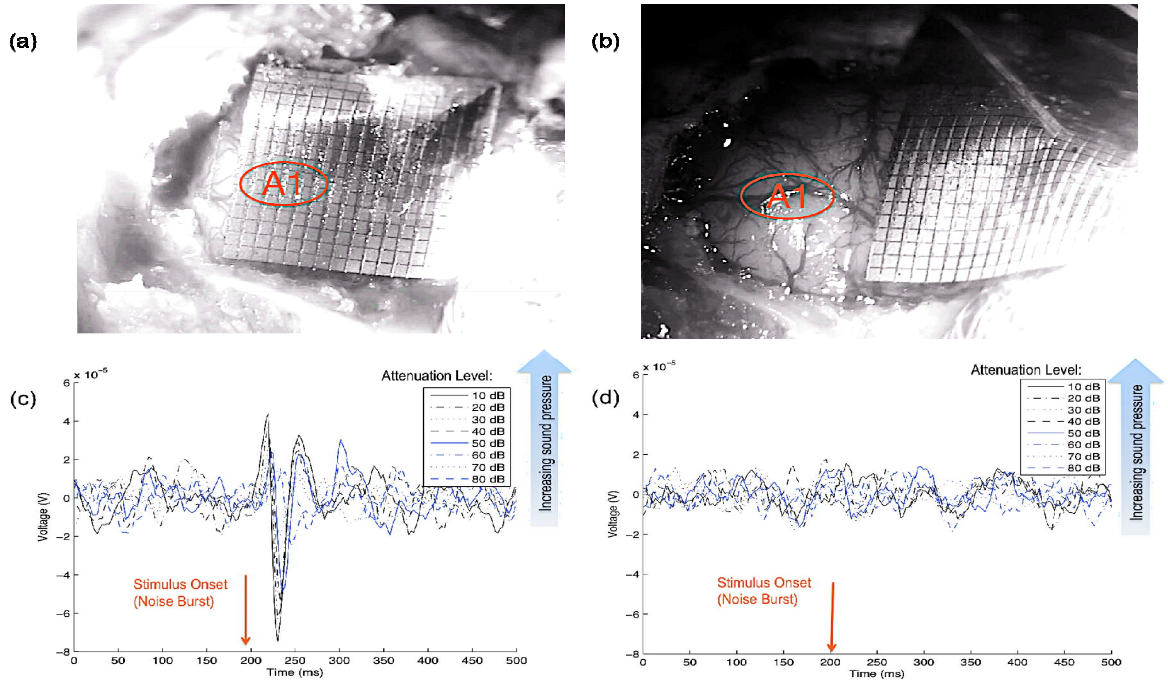

In vivo electrophysiology: (a) Grid placed on auditory cortex: Acoustic evoked potentials were observed approx. 30 ms after stimulus onset, at attenuations below 50 dB (c (b) Grid placed off auditory cortex for control purposes: No acoustic evoked potentials were observed under identical stimulation conditions (d). The red oval marked "A1" is the expected location of primary auditory cortex based on the presence of an auditory evoked response and its location relative to skull landmarks.

CONCLUSIONS AND FUTURE WORK

The reported device is a milestone towards BMIs based on high performance µECoG. The increased resolution will be useful for both novel communication prosthetics and as a means of addressing the outstanding issue of spatial sampling and electrode size for µECoG.

Increasingly the neuroscience community is recognizing the advantages of multiscale electrophysiological recordings [14]. To meet this need we are developing perforated ECoG arrays, which can be integrated with traditional penetrating microelectrode arrays such as the Utah array [15]. Such multiscale recordings will help elucidating the relationship between spikes, LFPs and µECoG-signals and likely enable higher-performing BMI decoders that combine information present on different length scales for decoding.

Beyond the development of multi-scale techniques, there is a wealth of opportunity in advanced technologies for µECoG systems. These include transparent electrodes for integration with modern optogenetic techniques, transitioning to roll-to-roll and polymer rapid prototyping technologies, the integration of on-polymer active electronics and wireless interfaces for long-term chronic recording in awake, behaving subjects.

ACKNOWLEDGEMENTS

The authors would like to thank Robert Knight, Dorian Liepmann, Christoph Schreiner, Jose Carmena, Edward Chang, ITO America Corp., and BSAC for funding, inspiring discussions and generous support of this work.

REFERENCES

[1] B. Rubehn, and T. Stieglitz, *Journal of neural engineering*, vol. 6, Jun. 2009, p. 036003.

[2] J. Kim and J.C. Williams, *IEEE Engineering in Medicine and Biology Society,* vol. 2007, Jan. 2007, pp. 5353-7.

[3] L.A. Geddes and C. Hodge, *IEEE Engineering in Medicine and Biology*, vol. 15, 1996, pp. 101-103.

[4] M. Stead and G.A. Worrell, *Brain : a journal of neurology*, vol. 133, Oct. 2010, pp. 2789-97.

[5] G.S. Brindley and M.D. Craggs, *The Journal of physiology*, vol. 223, May. 1972, p. 28P-29P.

[6] G. Schalk, *Frontiers in neuroengineering*, vol. 3, Jan. 2010, p. 9.

[7] J. Kubánek and G. Schalk, *Journal of neural engineering*, vol. 6, Dec. 2009, p. 066001.

[8] E.F. Chang and R.T. Knight, *Journal of cognitive neuroscience*, May. 2010.

[9] M.W. Slutzky and L.E. Miller, *Journal of neural engineering*, vol. 7, Apr. 2010, p. 26004.

[10] S. Katzner and M. Carandini, *Neuron*, vol. 61, Jan. 2009, pp. 35-41.

[11] E.O. Mann and O. Paulsen, *Neuron*, vol. 67, Jul. 2010, pp. 3-5.

[12] R.T. Canolty and J.M. Carmena, *Proceedings of the National Academy of Sciences*, vol. 107, Sep. 2010, pp. 17356-17361.

[13] N. Stark, *Medical Plastics and Biomaterials*, vol. 3, 1996, p. 30–35.

[14] B.H. Brinkmann, and M. Stead, *Journal of neuroscience methods*, vol. 180, May. 2009, pp. 185-92.

[15] P.K. Campbell and R.A. Normann, *IEEE transactions on bio-medical engineering*, vol. 38, Aug. 1991, pp. 758-68.